JOURNAL OF MATERIALS SCIENCE 32 (1997) 2391–2396

# Reduction of sodium-accelerated oxidation of silicon nitride ceramics by aluminium implantation

Y. CHEONG, H. DU
*Stevens Institute of Technology, Hoboken, NJ 07030, USA*
S. P. WITHROW
*Oak Ridge National Laboratory, Oak Ridge, TN 37831, USA*

Norton NBD 200 silicon nitride ceramics were implanted with sodium to a dose of $7.0 \times 10^{15} cm^{-2}$ at 72 keV (1 at% peak sodium content at 100 nm). The sodium-implanted samples were further implanted with aluminium to $7.3 \times 10^{15} cm^{-2}$ at 87 keV (1 at% peak aluminium content at 100 nm). The implanted and unimplanted samples were oxidized in 1 atm dry oxygen at 1100 and 1300 °C for 2–6 h. Profilometry and scanning electron microscopy measurements indicated that sodium implantation led to up to a two-fold increase in the oxidation rate of silicon nitride. The sodium effect was effectively neutralized when aluminium was co-implanted. The opposite effects of sodium and aluminium on the oxidation resistance of silicon nitride can be attributed to their different roles in modifying the structure and properties of the oxide formed.

## 1. Introduction

Sodium-accelerated oxidation of $Si_3N_4$ ceramics is a subject of extensive investigation owing to great technological interests in their use in industrial furnace and turbine engine environments, where sodium salts exist as common contaminants. A considerable amount of work has been done on the kinetics and mechanism of oxidation of various types of $Si_3N_4$ ceramics in the presence of sodium salts [1].

Pickrell *et al.* [2] reported that oxidation of commercial $Si_3N_4$ ceramics (Kyocera, SN220M) exhibited linear rates two to four orders of magnitude faster in dry air containing 0.98 vol% $NaNO_3$ vapor than in clean air or oxygen at 950–1100 °C. In a study employing the technique of ion implantation, Zheng *et al.* [3] showed that chemically vapour deposited (CVD) $Si_3N_4$, containing 0.1 at% uniformly implanted sodium, experienced a 14-fold increase over pure CVD $Si_3N_4$ in the parabolic oxidation rate constant in dry oxygen at 1100 °C. Experimental and thermochemical studies have illustrated that the process responsible for the accelerated oxidation of $Si_3N_4$ in the presence of various sodium salts is similar, despite some variation in details, regardless of the type and source of the sodium salts [1–5]. It can be generally stated that the sodium salts decompose to $Na_2O$ in an oxidizing environment which fluxes or dissolves the oxide formed. The resultant sodium silicates have poor network connectivity, low viscosity, low melting point, and high susceptibility to devitrification. The protective role of the oxide layer is diminished, leading to rapid transport of gaseous species, alteration of the oxidation mechanism, and oxidation acceleration. Sodium-accelerated oxidation is very detrimental because it facilitates other degradation processes which include pitting, nucleation of new flaw distributions, weakening of grain-boundary phases, and enhanced crack growth [6–8].

Based on the roles of $Na_2O$ and $Al_2O_3$ in glass forming in the $SiO_2$ system [9, 10], it is anticipated that aluminium surface alloying should provide an excellent prospect to negate the detrimental effect of sodium salts on the oxidation resistance of $Si_3N_4$. Using Norton NBD 200 $Si_3N_4$ as a test material, and ion implantation as a research vehicle, we demonstrated in the current study that aluminium surface alloying indeed offers a great potential for the improvement of the high-temperature oxidation resistance of $Si_3N_4$ in the presence of sodium. The results can be interpreted on the basis of modification of oxide network structure and thermodynamics of formation of silicates, which ultimately alter the mass transport and oxidation characteristics.

## 2. Experimental procedure

Commercial Norton NBD 200 $Si_3N_4$ was used in this investigation. This material is hot isostatically pressed with 1 wt% MgO as a sintering aid by Norton Advanced Ceramics, USA. Impurity elements present include carbon, aluminium, iron and calcium with respective compositions not exceeding 0.88, 0.5, 0.17 and 0.04 wt %. Platelets (10 mm × 10 mm × 3 mm) cut from the as-received $Si_3N_4$ blocks were polished to a 0.25 μm surface finish using diamond paste. The samples were ultrasonically cleaned in deionized

0022–2461  

water, acetone, and methanol prior to ion implantation experiments at Oak Ridge National Laboratory.

The platelet samples were implanted with sodium to a dose of $7.0 \times 10^{15}\,cm^{-2}$ at 72 keV. Some sodium-implanted samples were further implanted with aluminium to $7.3 \times 10^{15}\,cm^{-2}$ at 87 keV. These implantation parameters were selected using PROFILE simulation [11] in order to achieve a sodium and aluminium distribution each with 1 at % peak concentration at a projected range value of 100 nm. Samples were implanted at 500 °C to prevent implantation-induced amorphization [12, 13].

Oxidation experiments of the $Si_3N_4$ samples implanted with sodium and sodium/aluminium were carried out in a $MoSi_2$-heated $Al_2O_3$-tube furnace in 1 atm dry oxygen flowing at 100 standard $cm^3\,min^{-1}$ at 1100 and 1300 °C. The oxidation durations were 2, 4, and 6 h for each temperature condition. Unimplanted samples were simultaneously oxidized for comparison. To determine the oxide thickness, etch patterns were first created by brushing the sample with a photoresist (1-methoxy-2-propyl acetate) to mask selected areas of the oxide surface, oven baking at 130 °C for 30 min, and dipping in a buffered $NH_4F:HF$ (10:1) solution to remove the oxide not masked by the photoresist. The oxide thickness was determined by taking the average step height of the etch patterns using profilometry with a resolution of 25 nm. The samples were also investigated using scanning electron microscopy (SEM) to ascertain further the thickness of the oxide and to reveal its surface morphology. The oxidized samples were also characterized by energy-dispersive X-ray analysis (EDX) for compositional information and X-ray diffraction (XRD) for phase identification.

## 3. Results

### 3.1. Oxidation resistance

Shown in Fig. 1 is a computer-simulated sodium and aluminium concentration distribution in $Si_3N_4$ samples using the PROFILE codes [11]. PROFILE simulation gives results in good agreement with experimental values particularly in low to intermediate dose regions and when dopant redistribution during implantation is negligible as expected under the current implantation conditions [13]. The concentration profile is Pearson IV-type with a peak value of 1 at % for both sodium and aluminium at a depth of 100 nm beneath the sample surface. The profiles for sodium and aluminium nearly overlap with each other. This is advantageous because, according to Stevels' rule [9], aluminium addition in an amount equivalent to sodium is needed to eliminate completely sodium-induced non-bridging oxygens in $SiO_2$.

Shown in Fig. 2 are the profilometrical thickness of the oxide layers grown on unimplanted, sodium-implanted, and sodium/aluminium-implanted $Si_3N_4$ samples at 1100 °C for various durations. The results from 1300 °C oxidation are illustrated in Fig. 3. The

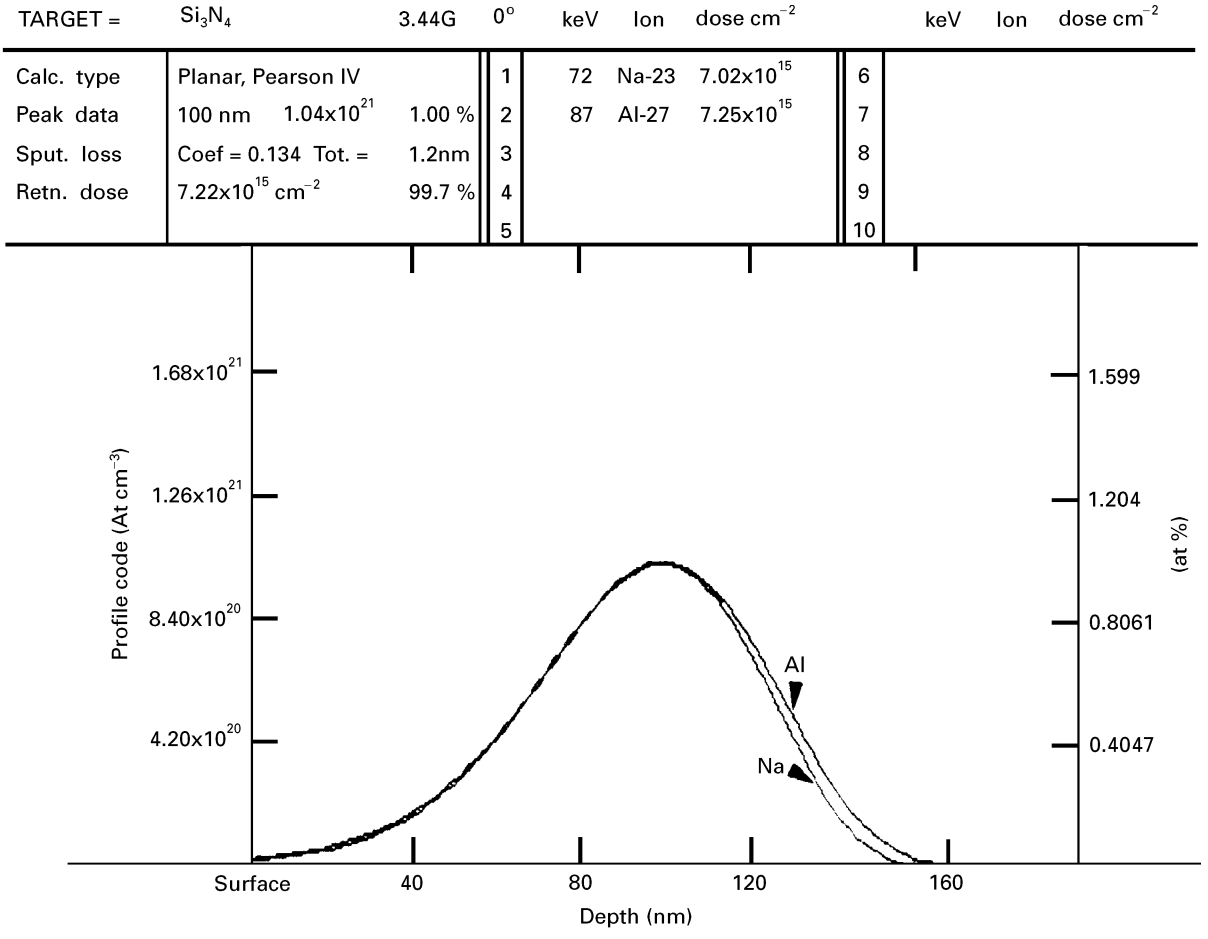


*Figure 1* Computer-simulated sodium and aluminium concentration distribution in $Si_3N_4$.

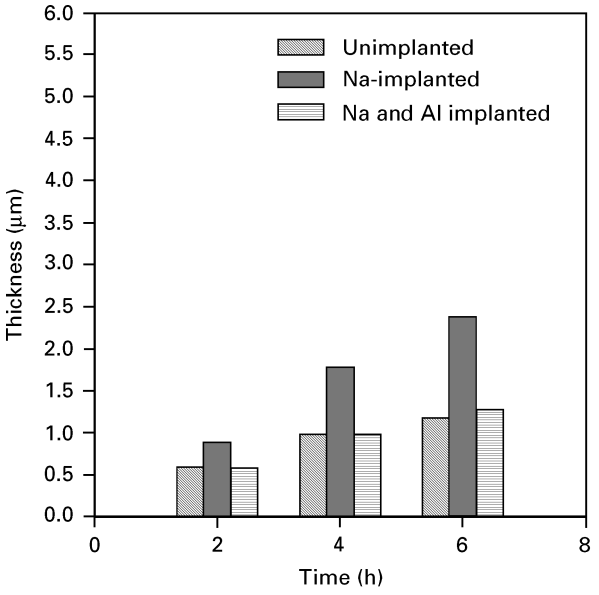


*Figure 2* Oxide thickness on unimplanted, sodium-implanted, and sodium/aluminium-implanted $Si_3N_4$ samples after oxidation at 1100 °C for various durations.

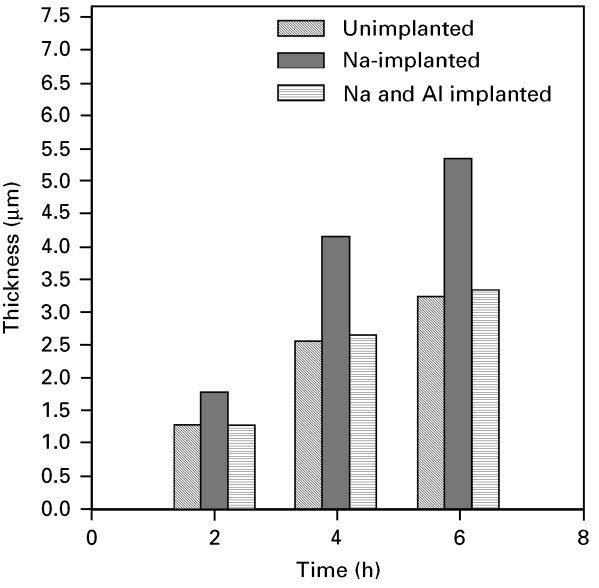


*Figure 3* Oxide thickness on unimplanted, sodium-implanted, and sodium/aluminium-implanted $Si_3N_4$ samples after oxidation at 1300 °C for various durations.

profilometrical thickness values are consistent with the thickness data measured using SEM. Illustrated respectively in Fig. 4a, b and c are tilt-angle scanning electron micrographs of unimplanted, sodium-implanted, and sodium/aluminium-implanted $Si_3N_4$ samples after 1300 °C/6 h oxidation and followed by pattern generation. The respective step height determined for these three samples is approximately 3.3, 5.0 and 3.6 μm, for example.

Figs 2 and 3 present a striking and consistent picture of the oxidation behaviour of the three types of $Si_3N_4$ samples; the presence of sodium led to up to a two-fold increase in the thickness of the oxide grown; the co-existence of sodium and aluminium produced no significant difference in the oxidation


*Figure 4* Tilt-angle scanning electron micrographs of (a) unimplanted, (b) sodium-implanted, and (c) sodium/aluminium-implanted $Si_3N_4$ samples after 1300 °C/6 h oxidation and pattern generation.

resistance compared with $Si_3N_4$ samples in the absence of sodium. A straight line can be drawn in Figs 2 and 3 to connect the thickness values of the oxide layers on sodium-implanted $Si_3N_4$. This line can be approximately extrapolated to the origin of the graph (zero thickness at zero time), an indication of a linear oxidation behaviour under the conditions employed in the current investigation. Such a trend is not

observed for data points from the unimplanted and sodium/aluminium-implanted $Si_3N_4$ samples.

## 3.2. Oxide characteristics

All samples, unimplanted or implanted, exhibited similar surface morphological characteristics after oxidation, regardless of temperature or duration. Figs 5a, b and c are scanning electron micrographs of unimplanted, sodium-implanted, and sodium/aluminium-implanted $Si_3N_4$ samples after 1300 °C/6 h oxidation. Oxidation led to no apparent surface roughening or bubble formation. SEM revealed the presence of numerous acicular phases in the oxide. The oxide layers experienced significant cracking in all cases investigated.

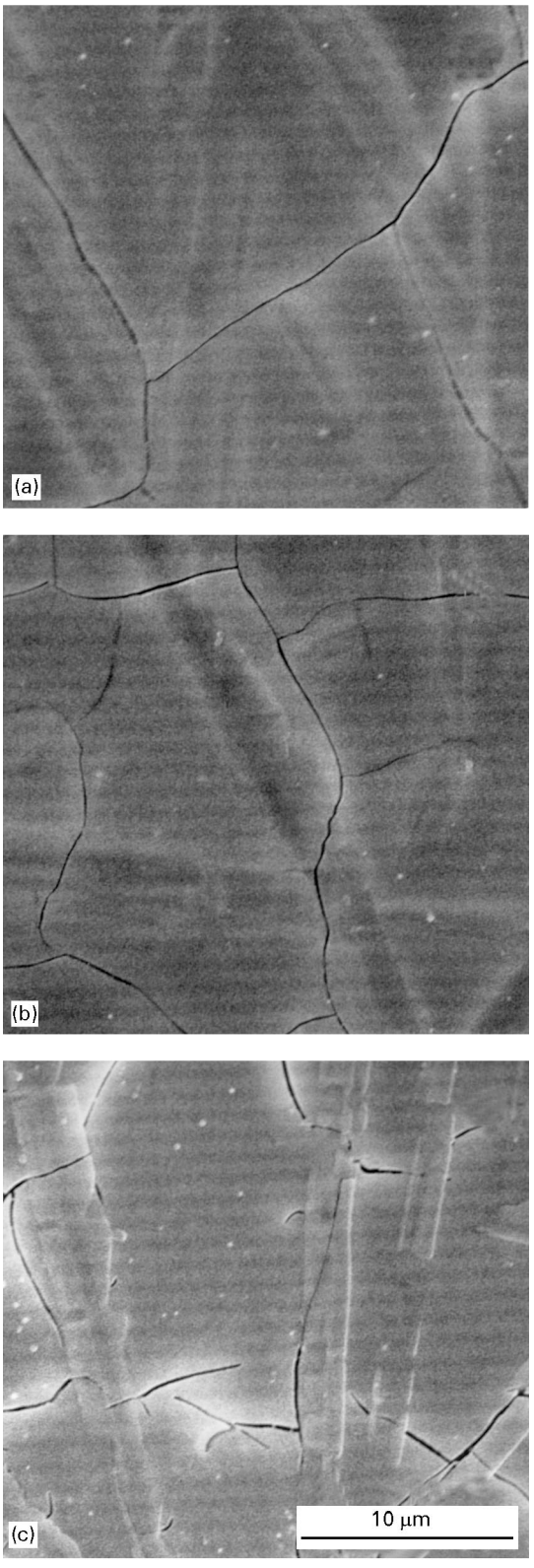


*Figure 5* Scanning electron micrographs of (a) unimplanted, (b) sodium-implanted, and (c) sodium/aluminium-implanted $Si_3N_4$ samples after 1300 °C/6 h oxidation.

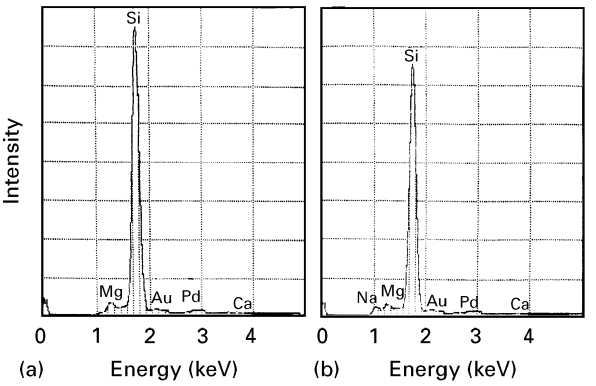


*Figure 6* EDX spectra from (a) the acicular phase and (b) a region away from the acicular phase of the oxide on sodium/aluminium-implanted $Si_3N_4$ samples after 1300 °C/6 h oxidation.

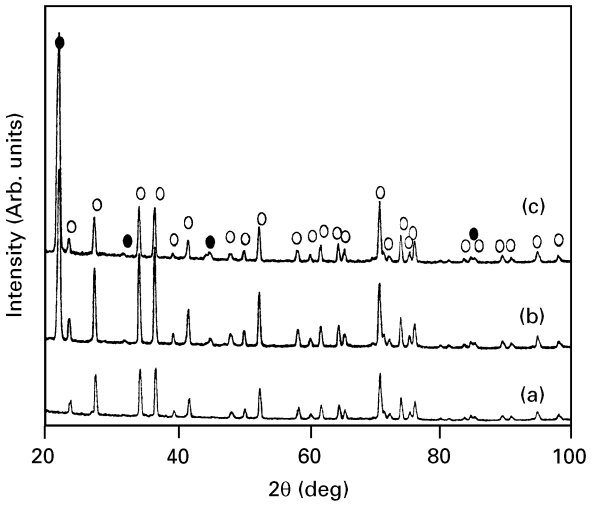


*Figure 7* XRD patterns of (a) as-received $Si_3N_4$, (b) unimplanted and (c) sodium/aluminium-implanted $Si_3N_4$ samples after 1300 °C/6 h oxidation. (●) Cristobalite $SiO_2$, (○) $\beta$-$Si_3N_4$.

The EDX work in current studies allowed some semi-quantitative evaluation of the oxidized samples. The oxides were enriched with magnesium with an average content of around 3 wt%. Shown in Fig. 6a, and b are the EDX spectra from an acicular phase and a region in its absence on sodium/aluminium-implanted $Si_3N_4$ samples after 1300 °C/6 h oxidation. Both magnesium and sodium were present in the bulk of the oxidation layer. In contrast, sodium was not detectable in the acicular phases embedded in the oxidation layer. Gold and palladium in the EDX spectra were from the overcoat applied to avoid sample charging during SEM analysis. The oxide layers on sodium-implanted $Si_3N_4$ exhibited similar characteristics. Owing to the abundance of silicon and

the low aluminium content in the system of investigation and the close proximity of these two elements in characteristic X-ray emission, information on aluminium could not be obtained in the current study.

Shown in Fig. 7a is an XRD pattern of as-received $Si_3N_4$. The corresponding diffraction peaks are denoted by open circles. The XRD patterns of the unimplanted and sodium/aluminium-implanted $Si_3N_4$ samples after 1300 °C/6 h oxidation are presented in Fig. 7b and c, respectively. In addition to diffraction peaks corresponding to the $Si_3N_4$ substrate, peaks, marked by solid circles, are present in the oxidized samples. The *d*-spacings of these peaks closely match those given by the JCPDS files for α-cristobalite [14]. The XRD results indicated that the oxide grown on the unimplanted and implanted $Si_3N_4$ samples is predominantly cristobalite.

## 4. Discussion

This investigation was not intended for a detailed study of the kinetics of oxidation of NBD 200 $Si_3N_4$, unimplanted and implanted. Oxidation evaluation was consequently limited to a few time durations. Early reports indicated that oxidation of $Si_3N_4$ hot-isostatically pressed with MgO as a sintering additive, follows a parabolic law in oxygen at 1000–1400 °C [15, 16]. Our data points (Figs 2 and 3) for unimplanted $Si_3N_4$ samples seemingly fall on such a trend line. There is a general agreement in the literature that oxidation of $Si_3N_4$ sintered with MgO is rate-controlled by outward diffusion of magnesium cations through the grain boundaries of the substrate into the oxide [1, 15, 16]. This consensus is drawn from the fact that the oxide is enriched with magnesium and no longer protective, and the oxidation rate is proportional to the MgO content in $Si_3N_4$.

The presence of sodium results in a significant change in the oxidation characteristics of $Si_3N_4$. As shown in Figs 2 and 3, sodium implantation led to up to a two-fold increase in the oxide thickness compared to the unimplanted case. More important, oxidation of the sodium-implanted samples exhibited a linear trend, suggesting a reaction- rather than diffusion-controlled mechanism. The sodium-induced rate increase and change of the oxidation mechanism can be interpreted according to the following.

The role of $Na_2O$ in silicate glass forming is well established [9, 10]. It is a network modifier and its incorporation into a silicate, such as $SiO_2$ and $MgSiO_3$, readily results in conversion of bridging oxygens to non-bridging oxygens. The formation of non-bridging oxygens is accompanied by deterioration in the network connectivity and degradation of a range of properties including lower viscosity, reduced eutectic temperature and accelerated mass transport [9, 10]. Rapid diffusion of magnesium cations in the oxide layer leads to fast removal of magnesium from the oxide/substrate interface. This process, in turn, increases the concentration gradient of magnesium between the oxide layer and the bulk grain-boundary phase, the driving force for outward diffusion of magnesium. Fast oxygen permeation through the oxide to the interface and large negative Gibb's free energies of formation of sodium and magnesium silicates [5, 17] also create a favourable condition for the silicate to be a sink of outward diffusion of magnesium. The in-take of magnesium cations, a network modifier, by the oxide further degrades the property of the oxide layer. As the rate of outward diffusion of magnesium increases, chemical reaction at the oxide/substrate interface will become rate-limiting.

The effect of aluminium addition is quite remarkable – nearly complete restoration of the oxidation resistance of sodium-implanted $Si_3N_4$ to that of unimplanted samples. From the glass-forming standpoint, $Al_2O_3$, an intermediate, plays a role significantly different from $Na_2O$ [9, 10]. For instance, $Al_2O_3$ can be integrated to the network structure of $SiO_2$ without interrupting the network connectivity. More important, its addition will eliminate non-bridging oxygens created by network modifiers in a silicate. In the current study, aluminium in an amount and distribution equivalent to sodium, was incorporated in the sodium-implanted $Si_3N_4$ samples. Under such a condition, according to Stevels' rule, no non-bridging oxygens will be created by sodium in the oxides grown on sodium/aluminium implanted samples. As a result, the afore-described adverse role of sodium in accelerating the outward diffusion of magnesium cations and altering the rate-limiting mechanism is negated. This outcome is clearly illustrated in Figs 2 and 3. On the basis of the current experimental observation and the underlying working concept, this is good reason to anticipate that an oxidation resistance better than that of the original material is achievable by implanting aluminium to a higher concentration than sodium, so as to compensate the detrimental effect of magnesium, besides sodium, on the properties of the oxide layers.

The nature of the oxide layer formed on $Si_3N_4$ containing various sintering additives and impurities has been shown to be complex [1, 15, 16] and is even more so with the sodium- and aluminium-implantation. The phases present include silicon dioxide, silicon oxynitride, and various silicates. The X-ray diffraction work indicated that the oxide formed is predominantly cristobalite (c-$SiO_2$). It is well established that the devitrification temperature of silica can be greatly reduced by additives and impurities (e.g. magnesium and sodium) via lowering its viscosity [18]. Cristobalite is the main cause of cracking of the oxide layers (Fig. 5) due to the large volume change associated with its β to α phase transformation during cooling [9].

Current X-ray analysis could not reveal the presence of other phases in the oxide due, probably, to their low contents. Magnesium enrichment in the oxide due to outward diffusion of magnesium cations from the substrate suggests probable formation of magnesium silicate. In fact, the morphological characteristics of the acicular phases in the oxide (Fig. 5) closely resemble those in documented studies of similar materials after oxidation, where they were positively identified to be enstatite ($MgSiO_3$) [15, 19].

## 5. Conclusions

1. The presence of sodium accelerates the oxidation process of NBD 200 $Si_3N_4$. Not only is the oxidation rate significantly increased, the oxidation mechanism is altered as well from a diffusion- to an interface reaction-controlled process.

2. The incorporation of aluminium effectively neutralizes the detrimental effect of sodium on the oxidation resistance of $Si_3N_4$ due to the role it plays in converting non-bridging oxygens created by sodium to bridging oxygens in the oxide.

3. Cristobalite is the predominant product phase during oxidation of $Si_3N_4$, unimplanted or implanted. Its phase transformation upon cooling is responsible for crack formation.

4. The current results have a broad implication in that the oxidation resistance of silica-forming ceramics under the influence of network modifiers (as additives or impurities) can be greatly enhanced by aluminium surface alloying.

5. Further work should focus on detailed kinetic studies and structural and chemical microanalysis to understand better the processes and mechanisms involved.


## Acknowledgements

This work was supported by the New Jersey Commission on Science and Technology. Work done at Oak-Ridge National Laboratory was funded by the US Department of Energy under contract DE-AC05-84OR21400 with Martin Marietta Energy Systems, Inc.


## References


1. N. S. JACOBSON, *J. Am. Ceram. Soc.* **76** (1993) 3.
2. G.R. PICKRELL, T. SUN and J. J. BROWN Jr, *Fuel Process. Technol.* **44** (1995) 213.
3. Z. ZHENG, R. E. TRESSLER and K. E. SPEAR, *Corr. Sci.* **33** (1992) 569.
4. M. J. MCNALLAN, P. P. HSU and S. Y. LEE, *JOM*, December (1993) 22.
5. N. S. JACOBSON, *Oxid. Metals* **31** (1989) 91.
6. K. G. NICKEL (ed.), "Corrosion of Advanced Ceramics, Measurement and Modelling", (Kluwer Academic, Dordrecht, The Netherlands, 1994).
7. R. E. TRESSLER and M. MCNALLAN (eds), "Corrosion and Corrosion Degradation of Ceramics", Ceramic Transactions, vol **10**, (The American Ceramic Society, Westerville, OH, 1990).
8. J. L. SMIALEK, D. S. FOX and N. S. JACOBSON, NASA-Lewis Research Center for the Environmental Degradation of Engineering Materials III, Report no. NASA TM-89820, NASA-Lewis Research Centre, Cleveland, OH, April 1987.
9. W. D. KINGERY, H. K. BOWEN and D. R. UHLMANN, "Introduction to Ceramics," 2nd Edn (Wiley, New York, 1976).
10. H. RAWSON, "Properties and Applications of Glass, Glass Science and Technology 3," (Elsevier Scientific, Amsterdam, 1980).
11. PROFILE codes, Implant Sciences Corp., Danvers, MA, USA.
12. Z. YANG, H. DU, M. LIBERA and I. L. SINGER, *J. Mater. Res.* **10** (1995) 1441.
13. H. DU, Z. YANG, M. LIBERA, D. JACOBSON, Y. C. WANG and R. F. DAVIS, *J. Am. Ceram. Soc.* **76** (1993) 330.
14. L. G. BERRY, B. POST, S. WEISSMANN and H. F. MCMURDIE (eds.) Powder Diffraction File (Inorganic Compounds) (Joint Committee on Powder Diffraction Standards, Swarthmore, PA, 1977).
15. S. C. SINGHAL, *J. Mater. Sci.* **11** (1976) 500.
16. D. CUBICCIOTTI and K. H. LAU, *J. Am. Ceram. Soc.* **61** (1978) 512.
17. A. PAUL, "Chemistry of Glasses", 1st Edn (Chapman and Hall, London, 1982).
18. E. T. TURKODOGAN and P. M. BILLS, *Am. Ceram. Soc. Bull.* **39** (1960) 682.
19. SHOJI NODA, HARUO DOI, TATSUMI HIOKI, JUNICHI KAWAMOTO and OSMAI KAMIKAITO, *J. Jpn. Soc. Powder Metall.* **35** (1988) 12.



*Received 23 February*
*and accepted 31 July 1996*